Sensors and Actuators A 165 (2011) 16–25

Contents lists available at ScienceDirect

Sensors and Actuators A: Physical

journal homepage: www.elsevier.com/locate/sna

Optimization and comparison of photonic crystal resonators for silicon microcantilever sensors

Trong Thi Mai[a,1], Fu-Li Hsiao[a,b,1], Chengkuo Lee[a,*,1], Wenfeng Xiang[a], Chii-Chang Chen[c], W.K. Choi[a,d]

[a] Department of Electrical and Computer Engineering, National University of Singapore, 4 Engineering Drive 3, Singapore 117576, Singapore
[b] Institute of Photonics, National Changhua University of Education, No. 1, Jin-De Road, Changhua City, 500 Taiwan, ROC
[c] Department of Optics and Photonics, National Central University, Jhongli, 320, Taiwan, ROC
[d] Advanced Materials for Micro- and Nano-Systems Programme, Singapore-MIT Alliance, Singapore 117576, Singapore

ARTICLE INFO

Article history:
Available online 11 January 2010

Keywords:
MEMS
NEMS
Photonic crystal resonator
Nano-ring
Nanomechanical sensor
Microcantilever

ABSTRACT

Microcantilever sensors have been known as a fundamental design used in force sensors, strain sensors and biochemical sensors. The fast-growing applications in nanoelectromechanical systems (NEMS) lead to strong demands in new sensing mechanism in order to downsize the sensing elements to nanometer scale. Photonic crystal (PC) based resonators have been investigated as promising solutions because the bandgap structure and resonator characteristics are extremely sensitive to the deformation and position shift of holes in PC resonators. In addition to the well-known nano-cavity resonator (NCR), we proposed hexagonal nano-ring resonators (NRR) of two different layout configurations. When a microcantilever under different force loads, both of the resonant wavelength and the resonant wavelength shift can be measured as a linear function of force load. The linear relationship between wavelength shifts and strain is observed as well. The minimum detectable force and detectable strain for NRR configuration 1 is derived as small as 0.0757 μN and 0.0023%. The outstanding sensing capability renders PC resonators as a promising nanomechanical sensing element to be integrated in various transducers for NEMS applications.

1. Introduction

Since the late 1980s there have been spectacular developments in micromechanical sensors and microelectromechanical systems (MEMS) which have enabled the exploration of transduction modes that involve mechanical energy and are based primarily on mechanical phenomena. Among these micromechanical transducers, microcantilever is a well-known and widely-adopted device. Microcantilever has been the fundamental sensor configuration for applications ranging from atomic force microscopy (AFM), force sensors, flow sensors, chemical and biological sensors, to actuators for dip-pen lithography [1–3]. The key feature distinguishing it from other sensor structures is its high sensitivity to beam deflection. The most common and commercially available method to measure the deflection of a cantilever is the so-called optical-lever technique using external bulky unit of laser-diode and position-sensitive photo diode detector [4]. In order to remove such a bulky laser testing unit, significant research effort has been devoted to the design and optimization of MEMS-based sensing mechanisms versus the cantilever shapes and dimensions. For example, the piezoresistive [5–6], the piezoelectric [7–12] and the capacitive [13] have been investigated extensively. Recently a suspended Si_3N_4 based microdisk resonator acting as a circular cantilever has been reported as a nanomechanical optical displacement sensor. A horizontal slot waveguide consisting of a Si_3N_4 based disk resonator is suspended and integrated on top of a silicon-based disk resonator, while a signal transmission Si waveguide is placed close to the Si_3N_4 disk resonator. When a downward bending of this circular cantilever modifies the local electromagnetic field, the modeling results have shown that the effective refractive index (ERI) change is a function of cantilever deflection. Such cantilever deflection can be potentially used as a sensing parameter for biosensors [14,15]. In view of the demands of using cantilevers for nanotechnology applications such as atomic manipulations, nanolithography and implanted biomedical devices, downsizing of cantilever and its strain sensing element, or cantilever deflection sensor, becomes a research task of great attention. As a result, nanoelectromechanical systems (NEMS) based sensors provide feasible approaches to enable smaller sensing elements.

Photonic crystals (PCs) are nanostructure materials in which a periodic variation of the material dielectric constant results in a photonic bandgap (PBG). This PBG effect of photonic crystals provides the highly confined mode needed to control the propagation of the light. In two-dimensional (2D) PCs, the electromagnetic field is localized in the defect region of periodic structure, e.g. line or

* Corresponding author. Tel.: +65 6516 5865; fax: +65 6779 1103.
E-mail address: elelc@nus.edu.sg (C. Lee).
[1] Shared the 1st authorship equally.

0924-4247/$ – see front matter © 2010 Elsevier B.V. All rights reserved.
doi:10.1016/j.sna.2010.01.006

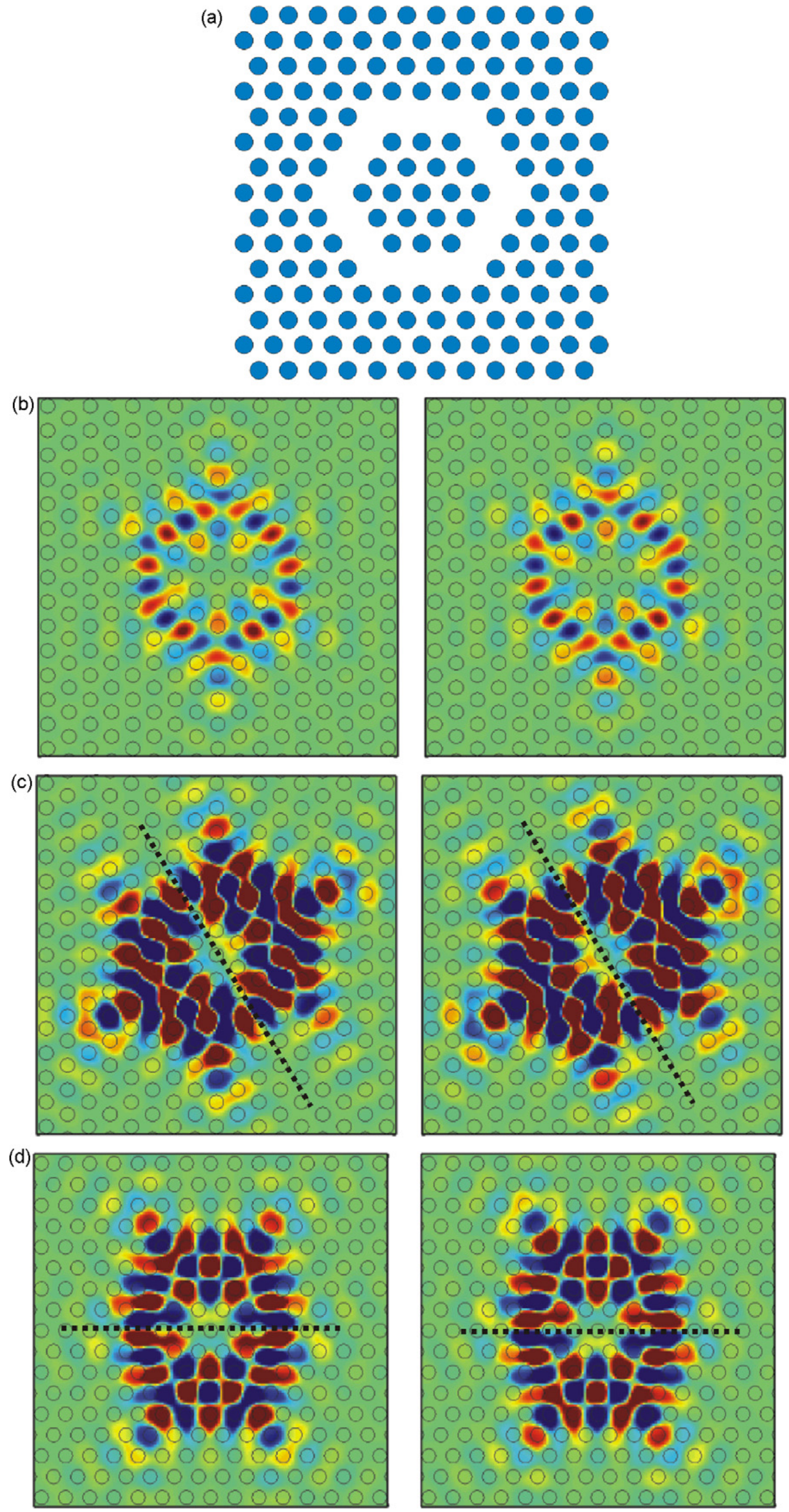

Fig. 1. (a) Layout configuration of a hexagonal nano-ring resonator. (b)–(d) Three types of resonant modes at 1561 nm. The degenerated modes are presented two abreast.

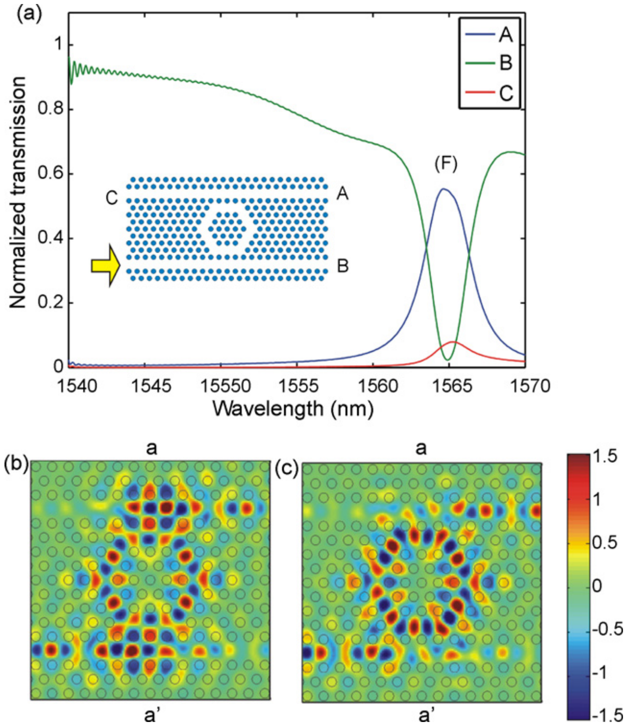

Fig. 2. (a) Spectra of ports A, B and C. (Inset) Sketch of channel drop filter with single resonator. The coupling distance is one line of air holes. (b) Real part of resonant steady out-of-plane magnetic field distribution. (c) Imaginary part of resonant steady out-of-plane magnetic field distribution.

point defect. The resonant cavity structures can be created by introducing point and/or line defects into 2D PC periodic holes array in which it supports field localization in PBG. Thus PC resonators exhibit resonant wavelength peak which is a function of the surface state of the defects, or the shape and dimension of the defects in the PC resonant cavity structures. A suspended silicon bridge beam structure integrated with PC waveguide nano-cavity based optical resonator has been investigated as a nanomechanical sensor [16]. The output resonant wavelength is sensitive to the shape of air holes and defect length of the nano-cavity resonator. When a strain is introduced by external force to the nano-cavity resonator of a pair of two-holes separated by a point defect, the resonant wavelength and shift of output resonant wavelength can be measured as the function of parameters such as displacement, strain or force. Later on, this sensing mechanism has been characterized as a NEMS sensor for microcantilevers of various dimensions operated in air and water environment [17–20]. A rather linear relationship is derived for strain and resonant wavelength shift. The minimum detectable strain and force load are observed as 0.0136% and 0.046 μN for a 50 μm long and 15 μm wide cantilever, [17]. On the other hand, two suspended InGaAsP PC beams with a thin air spacer layer in between have been proposed as a novel double-layered PC microcavity for force and stress sensors application [21]. It is a favorable approach for realization of multiple cantilever sensors by integrating PC lens, PC waveguides, or conventional waveguides, with 2D PC resonators to form a cascaded 1$\times$N microcantilever array which contains one PC resonator in an individual cantilever as the sensing element [17–20,22]. A pair of 2-hole located along a PC waveguide has been extensively characterized as nano-cavity PC resonators. In this paper, we investigated the sensing characteristics of a new nano-ring PC resonator and compared it with an existing PC resonator for microcantilever sensors.

2. Design and optimization of nano-ring resonators

Among the reported optical resonators, the circular micro-ring resonator of a few tens micrometers has been known as a good filter because it provides outstanding performances such as low loss, good confinement and high quality factor. The basic configuration of the micro-ring resonator comprises one or more ring waveguides and two straight waveguides along the two sides. A circulating resonant mode of micro-ring resonator is normally obtained by having the evanescent waves coupling between two bus waveguides and the micro-ring waveguides with regard to particular wavelengths fulfilling the constructive interference criteria, i.e., a function of micro-ring size. Although the micro-ring resonators have been reported as promising chemical sensors and mechanical sensors [23–25], precise control of spacing between waveguides and micro-ring, and dimension of the micro-ring are critical in order to achieve repeatable and reliable device characteristics [26]. The other type of microcavity based optical resonators such as micropillar cavity and whispering gallery microcavity have been investigated as force sensors and biochemical sensors as well [27–29]. K.J. Vahala has given a comprehensive overview on the microcavity resonators [29].

On the other hand, during the last decade, the rapid development of nanofabrication technology has enabled the successful demonstration of various PCs-based nano-cavity resonators [30]. Integration with suspended micro/nanostructures or actuators

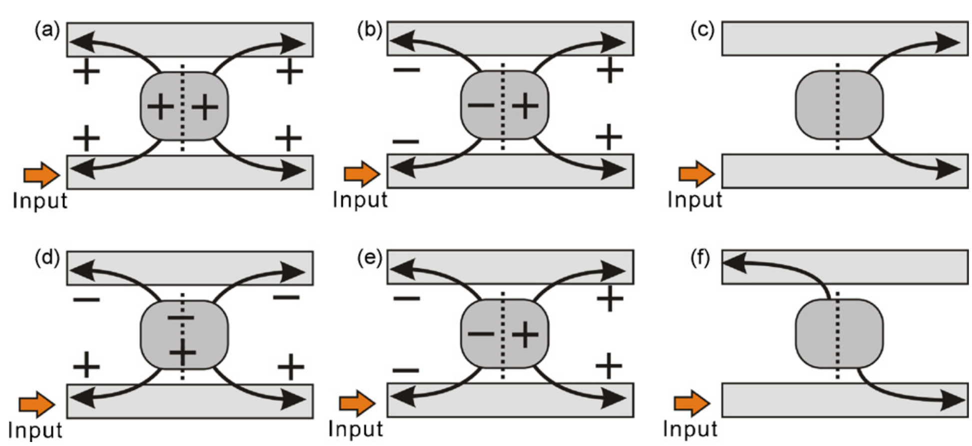

Fig. 3. (a)–(c) Sketch of the forward channel drop filter mechanism. The real part of resonant mode (a) is symmetric with respect to the mirror plane perpendicular to waveguide and the imaginary part of resonant mode (b) is anti-symmetric with respect to the mirror plane perpendicular to waveguide results in (c) forward drop. (d)–(f) Sketch of the backward channel drop filter mechanism. The real part of resonant mode (d) is symmetric with respect to the mirror plane parallel to waveguide and the imaginary part of resonant mode (e) is anti-symmetric with respect to the mirror plane perpendicular to waveguide results in (f) backward drop.

even gives tunability to resonators, i.e., tunable filters [31–33], or enables new functions [34]. In fact, PCs structures also provide an alternative ring resonator platform in nano-scale. Fan et al. [35] reported channel drop filters based on square-lattice 2D PCs. The resonators are consisted of one or two point defects inside the 2D PCs. The size and the refractive index of scatters are varied to match the desired resonance condition. The quality factor of forward and backdrop drop filters in their results is approximately 1000 and 6000, respectively. Qiang et al. [36] studied add-drop filters based on square-lattice PCs, thus the resonator comprises a square trace defect in 2D PCs. Four additional small air holes, i.e., scatters, are placed at the four corners of square defect to enhance the quality factor. The quality factor of single square ring filter is enhanced from 160 to over 1000 by increasing the coupling sections between waveguide and ring. They also proposed a dual-square-ring filter with quality over 2000. The drop direction and wavelength is decided by the relative position of the two rings. Recently Monifi et al. [37] presented a three output-ports channel drop filter based on the ring structure introduced by Qiang *et al.* in Ref. [36]. By manipulating the refractive index and radius of some scatters in PCs, they achieved a high transmission, three wavelengths channel drop filter in double-ring configuration. The estimated quality factor based on the reported data is about 100. PCs based ring resonators provide very well optical confinement due to ultra low bending loss. It is helpful to overcome the challenge aforementioned by reducing the radius of ring to achieve a resonator with high-Q, high wavelength selectivity, and ultra small footprint size. In addition, Hsiao and Lee reported a nano-ring resonator (NRR) based on 2D PC of

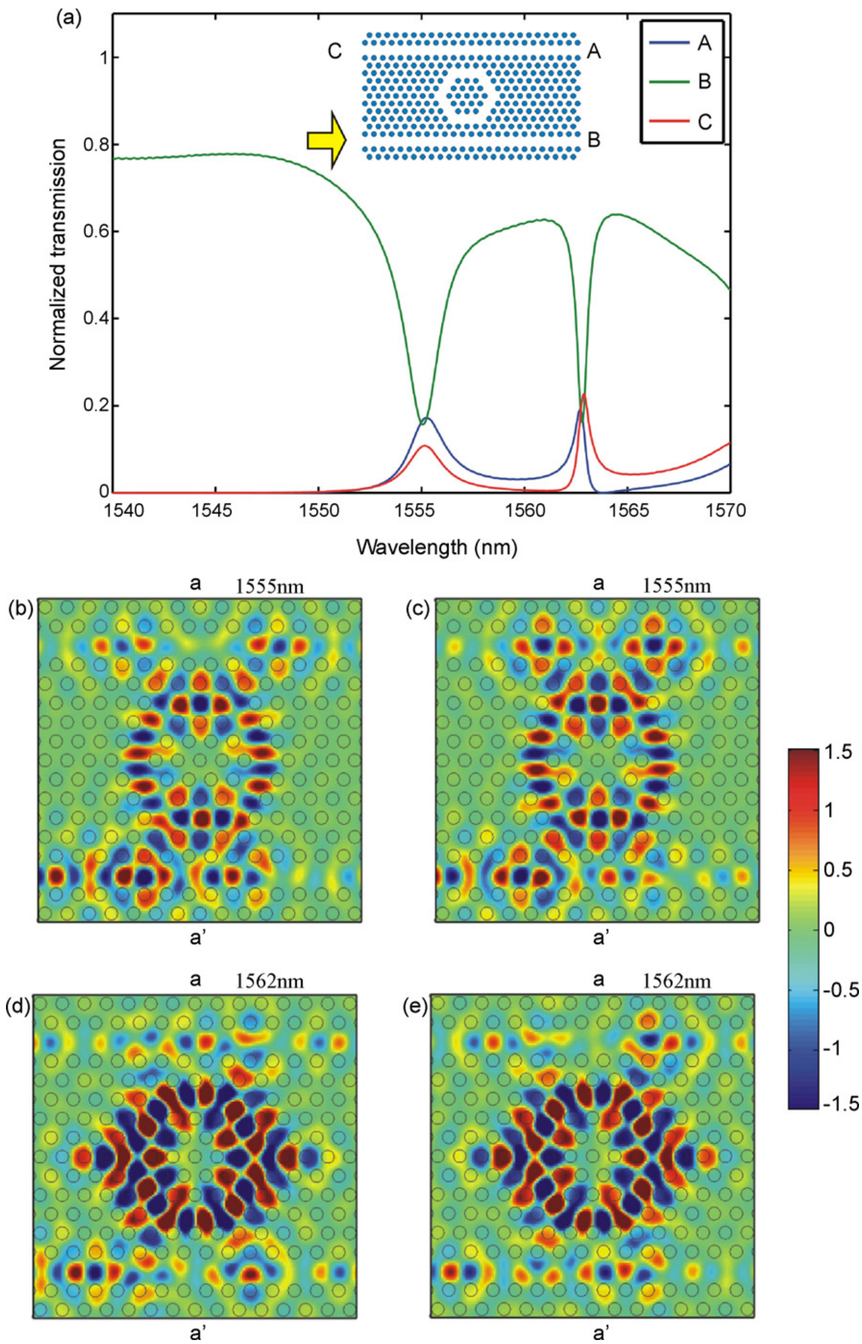

Fig. 4. (a) Spectra of ports A, B and C. (Inset) Sketch of channel drop filter with single resonator. The coupling distance is 2 lines of air holes. (b) Real part of resonant steady out-of-plane magnetic field distribution at 1555 nm. (c) Imaginary part of resonant steady out-of-plane magnetic field distribution at 1555 nm. (d) Real part of resonant steady out-of-plane magnetic field distribution at 1562 nm. (e) Imaginary part of resonant steady out-of-plane magnetic field distribution at 1562 nm.

hexagonal lattice [38]. The NRR structure is formed by removing holes cylinder along a hexagon in the 2D PC silicon slab as shown in Fig. 1 (a). By leveraging the excellent light confinement of PC slab structures, the NRRs demonstrate characteristics of resonators and filters as good as micro-ring resonators while its footprint has been significantly reduced to 1–4 μm. Owing to such promising characteristics of hexagonal NRRs, we are keen to explore the sensing characteristics in terms of force and strain for applications like microcantilevers.

In the section, we reported the design and optimization of NRR from the aspect of nanomechanical sensor applications. In Fig. 1(a), the ratio between the radius of air holes (r) and lattice constant (a) is selected as 0.292, while the lattice constant is 410 nm. The corresponding band gap wavelength range extends from 1305 nm to 1626 nm. Fig. 1(b)–(d) display three types of resonant modes at 1561 nm. The field distributions on the left and right, i.e., real and imaginary parts, are acquired in two different time frames. The time difference of these two frames is a quarter of the temporal period of the light. The mode in Fig. 1(b) is 6-fold symmetry. The symmetric axes in Fig. 1(c) and (d) are denoted as a dash line. Both modes observed in Fig. 1(c) and (d) are anti-symmetric with respective to the dash line. The above mentioned results have been derived by combining and using the two-dimensional finite-difference time-domain (2D FDTD) method and effective refractive index (ERI) approximation, while Qiu reported a good agreement between the data derived by this kind of combinational approach and full vector three dimensional (3D) FDTD method [39]. Kitamura et al. also reported that the cavity modes obtained by 2D plane wave expansion (PWE) method and ERI approximation in PC slab structure are in agreement with the measured results [40]. The effective refractive index of air/220 nm-Si/SiO_2 is derived as 2.82.

The inset in Fig. 2(a) illustrates the layout configuration of a channel drop filter with a hexagonal nano-ring which is sandwiched by two terminal waveguides with coupling distance (i.e., distance from the hexagonal nano-ring to the waveguide) of one line of air holes. The light input terminal on the left side of the bottom waveguide, i.e. the bus waveguide, is marked with a yellow arrow. Whereas the opposite side of the bottom waveguide, port B, is defined as the transmission terminal. Port A and C of the top waveguide are denoted as forward drop and backward drop terminals, respectively. The normalized spectra of the output-ports in A, B and C are displayed in Fig. 2(a) as green, blue and red lines, respectively. In the FDTD simulation, one lattice contents 20 spatial calculated grids. A temporal light pulse was incident into the input port. The time signal of each port is obtained by recording integration of the Poynting vector flow through the output cross-section of waveguide. The spectra are obtained by performing the Fast Fourier Transform (FFT) on the time-domain signals which are monitored at three ports and normalized to the transmission spectrum of pure line defect waveguide. The spectra show a strong resonant peak located at 1565 nm. The quality factor of forward dropping peak is 423. The energy in the bus waveguide are extracted by resonance at the hexagonal ring and coupled into port A (forward dropping). Fig. 2(b) and (c) display the steady out-of-plane magnetic field distribution in two different time frames. The steady field distribution is obtained by replace the temporal pulsed light source with a mono-wavelength temporally continued light source in FDTD simulation. The wavelength of the light source is set to be the resonant wavelength. The continued light source is launched into input waveguide until the field distribution is stable. The temporal phase difference between Fig.2(b) and (c) is 90°, i.e. a quarter of the temporal period of the light. This mode corresponds to Fig. 1(b) but with 4 nm wavelength shift. The slight discrepancy is caused by introducing the bus and drop waveguides. Adding waveguides on both sides of the NRR disturbs the boundary condition of resonance hence it results in the shifting of resonant wavelength.

In Fig. 2(a), we also observed that the intensity of forward dropping is stronger than backward dropping by a factor of 9. It has been reported that the asymmetric dropping mechanism can be explained by the symmetry of steady resonant field distribution of resonator [39]. In this model, the input wave is decomposed into real and imaginary parts. The asymmetric drop mechanism requests two conditions: (1) the real part and imaginary part couple into drop waveguide independently; (2) the spectral width and wavelength of resonance are equal for both parts. As Qiu reported in Ref. [39], the mechanism of asymmetric dropping into forward and backward ports in channel drop filter is depicted in Fig. 4. The forward drop cases are introduced in Fig. 3(a)–(c). The steady resonant field distributions in Fig. 2(a) and (b) reveal different symmetries with respect to the mirror plane which is perpendicular to waveguide (indicated by the dash line). The state decays to forward and backward directions with the same phase in Fig. 3(a) and exhibits 180° out of phase in Fig. 3(b). Hence the backward drop is totally cancelled. The backward drop can be explained by similar fashion via Fig. 3(d)–(f). The forward drop cancellation occurs when the symmetries of resonant modes of real and imaginary parts correspond to Fig. 3(d) and (e), respectively. On the other hand, due to the low symmetry of general channel drop system, only one-dimensional irreducible representation is allowed. An accidental degeneracy between the resonant modes of real and imaginary parts occurs when they belong to different irreducible representations. Thus, the input wave interferes destructively with the decaying wave of resonant mode into the forward direction of the bus waveguides [39]. In the FDTD computation, the real and imaginary parts of steady field distribution can be represented by the field distributions in two time steps with 90° temporal phase difference, i.e. Fig. 2(b) and (c). The steady out-of-plane magnetic field distributions in Fig. 2(b) and (c) are symmetric and anti-symmetric with respect to the mirror plane perpendicular to waveguide, as denoted as a virtual line of a–a′, respectively. According to the above mentioned cancellation mechanism of Fig. 3(a)–(c), this symmetry results in forward drop as observed in ports A and B in Fig. 2(a).

In order to enhance the quality factor, we increased the coupling distance to 2 lines of air holes as depicted in the inset of Fig. 4(a). Fig. 4(a) shows the normalized spectra of all output-ports. The resonant peaks split into two which are located at 1555 nm and 1562 nm. Fig. 4(b) and (c) show the real and imaginary parts of a steady out-of-plane magnetic field distribution of the resonance mode at 1555 nm whereas Fig. 4(d) and (e) show those of the resonance mode at 1562 nm. The quality factor for the peaks at 1555 nm and 1562 nm are 676 and 1690 respectively. The modes at 1555 nm and 1562 nm correspond to Fig. 1(b) and 1(c), respectively. The increased coupling distance leads to the disturbance of light wave coupling and confinement boundary condition. The corresponding wavelength of each resonance is shifted individually hence the resonant peak is split. Comparing with the resonant peak in Fig. 2(a), the quality factor is enhanced by increasing the coupling distance. We observed that, in both resonances, the light drop equally into forward and backward direction rather than only into forward direction as Fig. 3(a). In Fig. 4(b)–(e), both steady out-of-plane magnetic field distribution of real and imaginary parts are anti-symmetric with respect to the virtual line a-a'. The drop intensities into forward and backward directions are almost the same. In terms of sensing application, the configuration in Fig. 4(a) is more suitable than Fig. 2(a). First, the quality factor of configuration of Fig. 4(a) is higher and it means the sensitivity and resolution of sensing will be better. Second, the configuration of Fig. 4(a) enables the flexibility of the layout arrangement in order to meet various constraints attributed to multiple microcantilevers inside the fluidic channel. Since the drop light propagate into forward and backward direction equally such that both forward and backward drop ports could be adapted as the output signal for sensing applications.

3. Device configurations and modeling

Hexagonal NRR has been reported as a promising sensor with high wavelength selectivity and high quality factor [38]. To further exploit the potential sensor applications, three kinds of microcantilever sensors integrated with PC resonators are designed as shown in Fig. 5. The 50 μm long and 15 μm wide microcantilevers can be realized by removing the underneath bulk silicon from a silicon-on-insulator (SOI) substrate, while the released microcantilevers are bilayer beam and contain a 250 nm silicon layer on top of a 600 nm SiO_2 layer. In our previous studies [18,20], various microcantilever sensors with nano-cavity resonator (NCR) are studied (Fig. 5(a)), where the NCR is formed by having a pair of 2-hole located along a U-shaped PC waveguide. The lattice constant is $a = 540$ nm and the hole's radius $r = 220$ nm. The defect length, A_d, is defined as the distance between the second hole and the third hole of said 4-hole in the resonant cavity, and is given by $A_d = 2a - 2r$, as shown in inset of Fig. 5(a). To further investigate the performances of NRR-based micro cantilevers in term of force and strain detection, two kinds of NRR microcantilevers are proposed as shown in Fig. 5(b) and (c). The NRR is formed by a regular hexagonal array of air holes with lattice constant $a = 410$ nm and the radius of the holes $r = 120$ nm. Two bus PC waveguides are created by removing air holes along the two lines parallel to the edge of the hexagonal ring to form the input and output optical terminals. In order to investigate the resonant behavior of NRR under strain, we designed two types of NRR configurations. Fig. 5(b) shows the type 1 configuration (NRR1) which has a corner of the hexagon located at the edge of junction of the beam and the substrate, i.e., denoted as a dash line, and two bus PC waveguides arranged along the longitudinal direction of the microcantilever. We also define D_1 as

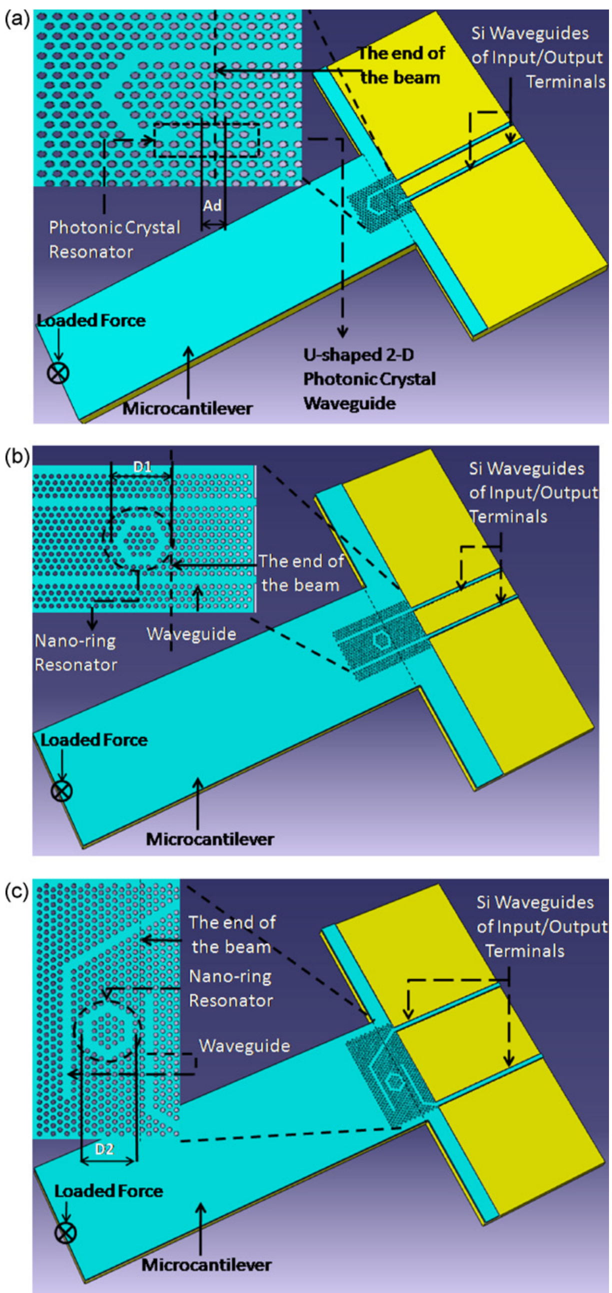

Fig. 5. 3D illustration of three types of microcantilever sensors using different PC resonator structure as strain sensors located at the edge of a Silicon-On-Insulator (SOI) chip. The silicon base was not shown in the figure but should be presented in the real device. (a) 4-holes PC resonator (b) Nano-ring resonator (Type1) (c) Nano-ring resonator (Type2).

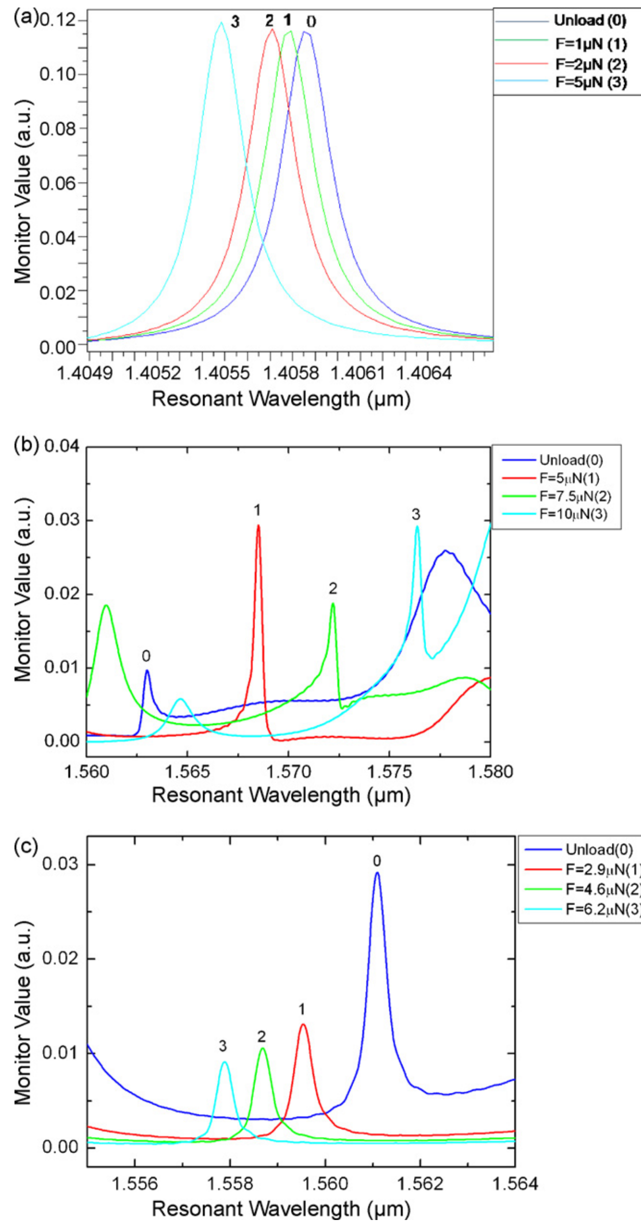

Fig. 6. Output of resonant peaks of the microcantilever sensors (a) Nano-cavity resonator (b) Nano-ring resonator (Type1) (c) Nano-ring resonator (Type2).

the NRR diameter which is the distance between the centers of the holes at the two vertexes of hexagonal ring along the longitudinal direction of the microcantilever. On the other hand, type 2 configuration (NRR2) shown in Fig. 5(c) depicts that an edge of hexagonal ring is along the edge of junction of the beam and the substrate, and two bus PC waveguides arranged along or parallel to this substrate edge. Meanwhile, we define D_2 as the NRR diameter which is the distance between the centers of the holes adjacent to two edges of the hexagonal ring along the edge of the fixed end of the microcantilever. According to the configuration shown in Fig. 2 and Fig. 4, the output terminal of NRR1 and NRR2 collects the backward drop and forward drop signals, respectively.

The modeling involves with two parts. First of all, a finite-element method (FEM) simulation is carried out to get the deformation contour of holes of the PC resonator under various force loads. As shown in Fig. 5, this force is applied at the center of microcantilever end and makes it bend downward. In the modeling, the Young's modulus and Poisson's ratio of Si and SiO_2 are 130 GPa, 70 GPa, 0.3 and 0.17, respectively. Second, a 2D FDTD simulation is used to get the characteristics of the resonators under various strains. The effective refractive index used in the modeling is derived as the Si/SiO_2 bilayer microcantilevers operated in air. Among the output spectra of resonators under various force loads, we only select the peaks attributed to resonant modes of resonators. The backward drop and forward drop signals are recorded for NRR1 and NRR2 sensors respectively.

4. Characterization of sensors

Fig. 6(a)–(c) shows various simulated resonant wavelength peaks of these microcantilever sensors under no loading condition and three different loading forces. For NCR sensor, the loaded forces are chosen as 1 μN, 2 μN and 5 μN. In the case of NRR1, forces of 5 μN, 7.5 μN and 10 μN are picked. For NRR2, the force magnitudes are selected as 2.9 μN, 4.6 μN and 6.2 μN. Observations show that as the loaded force increases, in the case of NCR and NRR2, the resonant peak shifts to a shorter wavelength region, i.e. a blue shift. Contrarily, the resonant peak shifts to a longer wavelength region for NRR1, i.e. a red shift. The behavior of resonant wavelength shift of NRR1 and NRR2 may be resulted from the different shape change of the NRR structure. Under loading forces, the beam deflection causes the changes in both the relative positions with respect to the fixed end and the shape of the air holes. FEM results have shown that the change in the shape, i.e. the radius of the holes is very small compared to the change in position (in the order of one tenth). For instance, in NRR1, when the position shifts 76.5 nm, the radius changes merely by 5.77 nm. Therefore the air hole radius change is negligible in 2D FDTD calculation. However, the position change of a hole depends on the specific location of this hole and the layout configuration of the resonator placed at the edge of the cantilever fixed end. When the force is exerted in the z-direction, in the case of NRR1, the air holes shift in the direction parallel to the waveguide such that the hexagonal ring becomes more oval-shaped. When the light is provided into NRR1, the longer wavelength resonant mode will be coupled into the hexagonal ring. As a result, we observed a red shift. In the case of NRR2 structure, the air holes move perpendicularly to the waveguide so as to make the hexagonal ring close to a square ring. The longer resonant mode will be limited and only the shorter wavelength resonant mode can be coupled into NRR2. Thus the blue shift trend is observed in Fig. 6(c). On the other hand, for NCR structure, we have reported that the resonant wavelength shift is mainly attributed to the change of defect length A_d [16–17,20].

Fig. 7(a)–(c) show the wavelength of resonant peaks of these three kinds of microcantilever sensors as a function of the loaded force. Linear relationship is observed for the variation of resonant peaks regarding to different loaded forces. The no-load resonant peaks for NCR, NRR1 and NRR2 microcantilevers are determined to be at 1405.87 nm, 1562.99 nm and 1561.10 nm, respectively. Besides, Table 1 shows the quality factor of resonant peaks of these microcantilever sensors. It is observed that the quality factor of resonant peaks show variation less than 10% under various loaded force. Essentially the quality factor of NCR, NRR1 and NRR2 is about 5500, 3500 and 3800, respectively. The quality factor of NRR2 is slightly larger than that of NRR1 because forward drop signal typically has higher quality factor than backward drop signal.

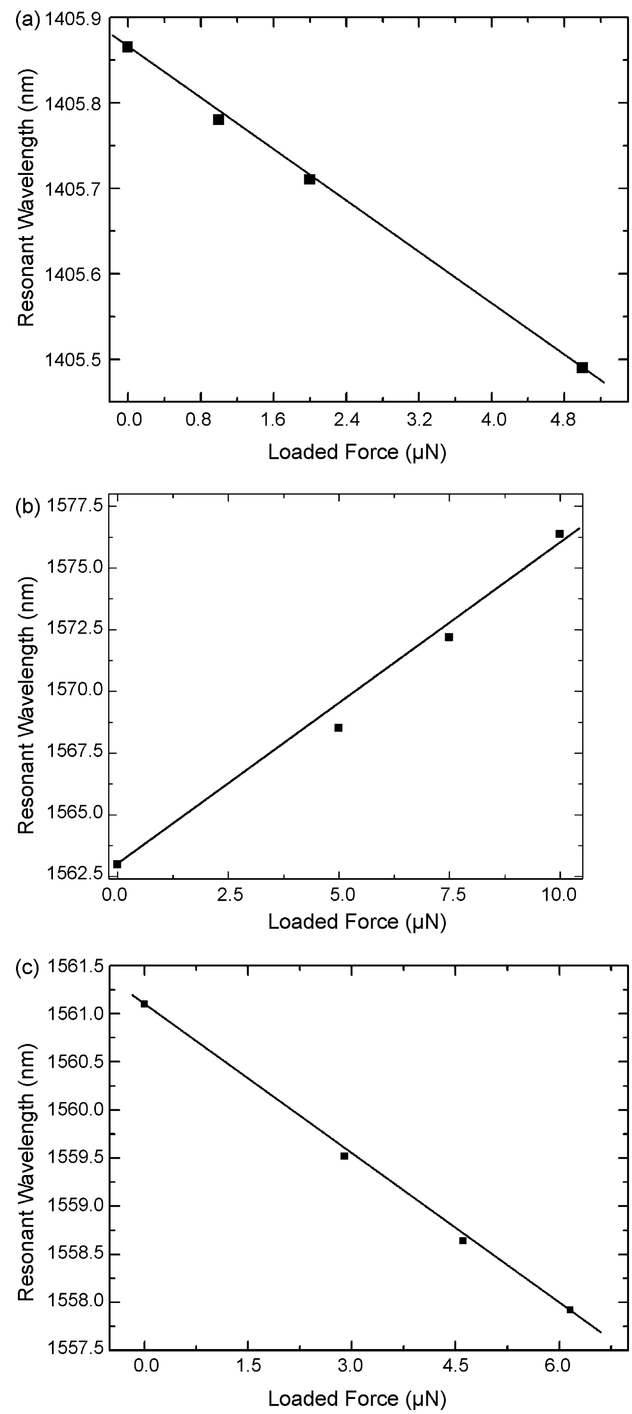

Fig. 7. Resonant wavelength versus the loading force. (a) Nano-cavity resonator (b) Nano-ring resonator (Type1) (c) Nano-ring resonator (Type2).

Table 1
Quality factor versus loaded force.

NCR		NRR1		NRR2	
Force (μN)	Q-factor	Force (μN)	Q-factor	Force (μN)	Q-factor
0	5223.16	0	3896.85	0	4077.68
1	5508.54	5	3508.96	2.89809	3597.76
2	5513.84	7.5	2962.05	4.60877	3931.88
5	5522.55	10	3520.00	6.16079	3783.11

As shown in Fig. 8, the resonant wavelength shift is plotted as the function of the loaded force. With respect to 0.1 nm wavelength shift resolution, the minimum detectable force for NRR1 and NRR2 are derived as 0.0757 μN and 0.1299 μN in that order, compared with 1.3461 μN for NCR. It can be seen that the better

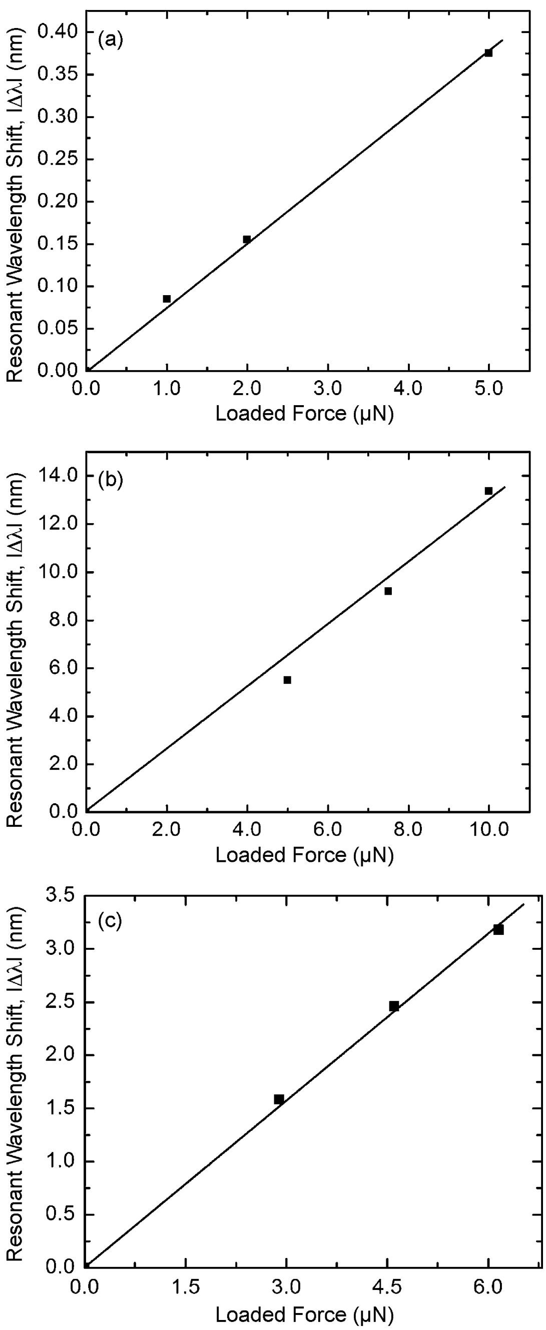

Fig. 8. Resonant wavelength shift versus the loading force. (a) Nano-cavity resonator (b) Nano-ring resonator (Type1) (c) Nano-ring resonator (Type2).

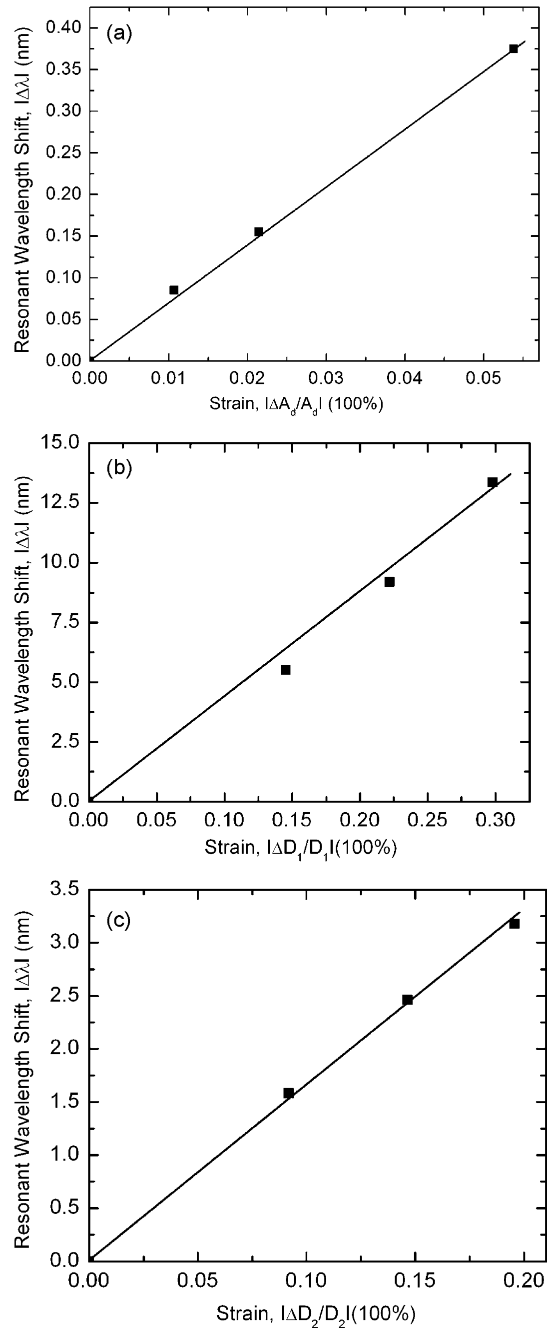

Fig. 9. Resonant wavelength shift versus the strain. (a) Nano-cavity resonator (b) Nano-ring resonator (Type1) (c) Nano-ring resonator (Type2).

detection limit of force is the NRR1. It is attributed to a larger wavelength shift at the same load force compared to the other cases. For instances, when the force increases from 0 μN to 5 μN, the resonant wavelength shifts from 1562.99 nm to 1568.50 nm, i.e. a resonant wavelength shift ($\Delta\lambda$) of 5.5 nm. In contrast to NRR1, $\Delta\lambda$ of NCR is only 0.3755 nm for 5 μN force load increment, i.e., from 1405.87 nm to 1405.49 nm, while $\Delta\lambda$ of NRR2 is about 3.18 nm regarding to 6.1 μN force load increment, i.e., from 15611.00 nm to 1557.92 nm.

The strain is defined as the percentage change in length of active area of resonators. As a result, we have $\Delta A_d/A_d$, $\Delta D_1/D_1$, and $\Delta D_2/D_2$ for the NCR, NRR1 and NRR2, respectively. According to the FEM results, we can calculate the strains under different force loads. With the data of $\Delta\lambda$ versus force loads in Fig. 8, we can plot $\Delta\lambda$ versus strain in Fig. 9. Again, a linear relation is observed between $\Delta\lambda$ and strain for NCR and NRR. Using this linear line, the minimum detectable strain can be derived as 0.0144%, 0.0023% and 0.0041% for NCR, NRR1, and NRR2, respectively, regarding to 0.1 nm wavelength resolution. Therefore, NRR1 also surpass the other two resonators in term of sensitivity of strain detection.

In brief, this new type nanosensor based on NRR shows promising potential in applications like force sensing and strain detection. In contrast to the approach discussed in micro-ring resonator based displacement sensor which detect the intensity variation of resonant peak [28], our approach works on the detection of resonant wavelength shift such that our devices are less susceptible to fundamental noises. Additionally the size of NRR is only 3–10% of the total size of the micro-ring resonator [28]. It implies NNR sensor will be favored as a feasible sensing approach in nano-scale and integrated on nanostructures for various applications in future.

5. Conclusions

In this paper, we have investigated Si/SiO_2 bilayer microcantilevers integrated with photonic crystal based Si resonators as force and strain sensors. In addition to the well-known nano-cavity resonator (NCR), we proposed the hexagonal nano-ring resonator in two layout configurations. Both the resonant wavelength and the resonant wavelength shift can be measured as a linear function of force load. For the NCR and NRR2, the resonant peaks exhibit blue shift phenomena. On the contrary, the resonant peak of NRR1 moves to the longer wavelength region, i.e. the red shift. To quantify the strain sensing capability, the percentage change in length of active area of resonators is defined as the strain. The linear relationship between wavelength shifts and strain is observed for both microcantilevers integrated with NRR1 and 2, while such linear relationship has been reported for NCR sensors by authors in previous studies. This linear response behavior enables the proposed structures to be very promising for sensing applications. The minimum detectable force for NCR, NRR1 and NRR2 are 1.3461 μN, 0.0757 μN, and 0.1299 μN respectively. The minimum detectable strain for NRR1 and NRR2 are 0.0023% and 0.0041% compared with 0.0144% for NCR. Compared to the properties of NCR and NRR2, the NRR1 has the better detected ability of the strain and force. However, the quality factor of resonant peaks of NRR1 is slightly lower than that of NCR and NRR2.

Acknowledgement

This work was supported in research grants of University Research Fund R-263-000-475-112 at the National University of Singapore, and A-STAR, SERC Grant No. 0921010049. Authors thank valuable advice from Prof. Aaron Danner and Prof. Gengchiau Liang. Authors also thank the technical support from staff at Computational Nanoelectronics & Nanodevices Lab., Microelectronics Lab., Centre for Integrated Circuit Failure Analysis & Reliability (CICFAR), and Centre for Optoelectronics of National University of Singapore.

References

[1] N.V. Lavrik, M.J. Sepaniak, P.G. Datskos, Cantilever transducers as a platform for chemical and biological sensors, Rev. Sci. Instrum. 75 (2004) 2229–2253.
[2] C. Ziegler, Cantilever-based biosensors, Anal. Bioanal. Chem. 379 (2004) 946–959.
[3] D.S. Ginger, H. Zhang, C.A. Mirkin, The evolution of dip-pen nanolithography, Angew. Chem. Int. Ed. 43 (2004) 30–45.
[4] G. Meyer, N.M. Amer, Novel optical approach to atomic force microscopy, Appl. Phys. Lett. 53 (1988) 1045–1047.
[5] M. Tortonese, R.C. Barrett, C.F. Quate, Atomic resolution with an atomic force microscope using piezoresistive detection, Appl. Phys. Lett. 62 (1993) 834–836.
[6] P.A. Rasmussen, J. Thaysen, O. Hansen, S.C. Eriksen, A. Boisen, Optimized cantilever biosensor with piezoresistive read-out, Ultramicroscopy 97 (2003) 371–376.
[7] T. Itoh, C. Lee, T. Suga, Deflection detection and feedback actuation using a self-excited piezoelectric $Pb(Zr,Ti)O_3$ microcantilever for dynamic scanning force microscopy, Appl. Phys. Lett. 69 (1996) 2036–2038.
[8] C. Lee, T. Itoh, R. Maeda, T. Ohashi, T. Suga, Development of a piezoelectric self-excitation and self-detection mechanism of PZT microcantilevers for dynamic SFM in liquid, J. Vac. Sci. Technol. B 15 (1997) 1559–1563.
[9] J. Chu, T. Itoh, C. Lee, T. Suga, K. Watanabe, Frequency modulation detection high vacuum scanning force microscope with a self-oscillating piezoelectric cantilever, J. Vac. Sci. Technol. B 15 (1997) 1647–1651.
[10] C. Lee, T. Itoh, T. Suga, Self-excited piezoelectric PZT microcantilevers for dynamic SFM-with inherent sensing and actuating capabilities, Sens. Actuators, A 72 (1999) 179–188.
[11] W. Dong, X. Lu, M. Liu, Y. Cui, J. Wang, Measurement on the actuating and sensing capability of a PZT microcantilever, Meas. Sci. Technol. 18 (2007) 601–608.
[12] S. Shin, J.P. Kim, S.J. Sim, J. Lee, A multisized piezoelectric microcantilever biosensor array for the quantitative analysis of mass and surface stress, Appl. Phys. Lett. 93 (2008) 102902.
[13] J. Brugger, R.A. Buser, N.F. de Rooij, Micromachined atomic force microprobe with integrated capacitive readout, J. Micromech. Microeng. 2 (1992) 218–220.
[14] C.A. Barrios, Ultrasensitive nanomechanical photonic sensor based on horizontal slot waveguide resonator, IEEE Photon. Technol. Lett. 18 (2006) 2419–2421.
[15] K.S. Hwang, S.-M. Lee, S.K. Kim, J.H. Lee, T.S. Kim, Micro- and nanocantilever devices and systems for biomolecule detection, Annu. Rev. Anal. Chem. 2 (2009) 77–98.
[16] C. Lee, R. Radhakrishnan, C.C. Chen, J. Lin, J. Thillaigovindan, N. Balasubramanian, Design and modeling of a nanomechanical sensor using silicon photonic crystals, J. Lightwave Technol. 26 (2008) 839–846.
[17] C. Lee, J. Thillaigovindan, C. Chen, X.T. Chen, Y. Chao, S. Tao, W. Xiang, A. Yu, H. Feng, G.Q. Lo, Si nanophotonics based cantilever sensor, Appl. Phys. Lett. 93 (2008) 113113.
[18] W. Xiang, F.-L. Hsiao, C. Lee, Microcantilever sensor using photonic crystal nano-cavity resonator, in: 15th International Conference On Solid-State Sensors, Actuators and Microsystems, IEEE Transducers'09, June 21–25, 2009 Denver, USA, 2009, pp. 959–962.
[19] C. Lee, J. Thillaigovindan, Optical nanomechanical sensor using a silicon photonic crystals cantilever embedded with a nano-cavity resonator, Appl. Opt. 48 (2009) 1797–1803.
[20] W. Xiang, C. Lee, Nanophotonics sensor based on microcantilever for chemical analysis, IEEE J. Sel. Top. Quantum Electron. 15 (2009) 1323–1326.
[21] T.-W. Lu, P.-T. Lee, Ultra-high sensitivity optical stress sensor based on double-layered photonic crystal microcavity, Opt. Express 17 (2009) 1518–1526.
[22] H.-T. Chien, C. Lee, H.-K. Chiu, K.-C. Hsu, C.-C. Chen, J.-A.A. Ho, C. Chou, The comparison between the graded photonic crystal coupler and various couplers, IEEE J. Lightwave Technol. 27 (2009) 2570–2574.
[23] C.Y. Chao, W. Fung, L.J. Guo, Polymer micro-ring resonators for biochemical sensing applications, IEEE J. Sel. Top. Quantum Electron. 12 (2006) 134.
[24] K. de Vos, I. Bartolozzi, E. Schacht, P. Bienstman, R. Baets, Silicon-on-insulator micro-ring resonator for sensitive and label-free biosensing, Opt. Express 15 (2007) 7610–7615.
[25] I. Kiyat, C. Kocabas, A. Aydinli, Integrated micro-ring resonator displacement sensor for scanning probe microscopies, J. Micromech. Microeng. 14 (2004) 374–381.
[26] C.B.E. Little, J.P. Laine, S.T. Chu, Surface-roughness-induced contradirectional coupling in ring and disk resonators, Opt. Lett. 22 (1997) 4–6.
[27] T. Ioppolo, M. Kozhevnikov, V. Stepaniuk, M.V. Ötügen, V. Sheverev, Micro-optical force sensor concept based on whispering gallery mode resonators, Appl. Opt. 47 (2008) 3009–3014.
[28] A.M. Armani, R.P. Kulkarni, S.E. Fraser, R.C. Flagan, K.J. Vahala, Label-free, single-molecule detection with optical microcavities, Science 317 (2007) 783–786.
[29] K.J Vahala, Optical microcavities, Nature 424 (2003) 839–846.
[30] P. Lalanne, C. Sauvan, J.P. Hugonin, Photon confinement in photonic crystal nanocavities, Laser Photon Rev. 2 (2008) 514–526.
[31] T. Baba, Slow light in photonic crystals, Nat. Photonics 2 (2008) 465–473.
[32] I. Favero, K. Karrai, Optomechanics of deformable optical cavities, Nat. Photonics 3 (2009) 201–205.
[33] Y. Kanamori, K. Takahashi, K. Hane, An ultrasmall wavelength-selective channel drop switch using a nanomechanical photonic crystal nano-cavity, Appl. Phys. Lett. 95 (2009) 171911.
[34] I.W. Jung, S.B. Mallick, O. Solgaard, A large-area high-reflectivity broadband monolithic single-crystal-silicon photonic crystal mirror MEMS scanner with low dependence on incident angle and polarization, IEEE J. Sel. Top. Quantum Electron. 15 (2009) 1447–1454.
[35] S. Fan, P.R. Villeneuve, J.D. Joannopoulos, H.A. Haus, Channel drop filters in photonic crystals, Opt. Express 3 (1998) 4–11.
[36] Z. Qiang, W. Zhou, R.A. Soref, Optical add-drop filters based on photonic crystal ring resonators, Opt. Express 15 (2007) 1823–1831.
[37] F. Monifi, A. Ghaffari, M. Djavid, M.S. Abrishamian, Three output port channel drop filter based on photonic crystals, Appl. Opt. 48 (2009) 804–809.
[38] F.-L. Hsiao, C. Lee, Novel Hexagonal Nano-ring Resonator, in: IEEE NANO 2009, Genoa, Italy, July 26–30, 2009, pp. 263–366.
[39] M. Qiu, Effective index method for the heterostructure-slab-waveguides-based two-dimensional photonic crystals, Appl. Phys. Lett. 81 (2002) 1163.
[40] M. Kitamura, S. Iwamoto, Y. Arakawa, Enhanced light emission from an organic photonic crystal with a nano-cavity, Appl. Phys. Lett. 87 (2005) 151119.

Biographies

Trong Thi Mai received the B.Sc. degree from the Department of Electrical and Computer Engineering at the National University of Singapore in 2009. He is currently working toward a PhD degree at the same university

Fu-Li Hsiao received the B.S. degree in the Department of Physics of National Changhua University of Education, Taiwan, in 2002 and the PhD. degree in FEMTO-ST of University of Franche-Comte, France, and in Department of Optics and Photonics of National Central University, Taiwan, in 2008. He has been a post-doctoral research fellow in the Department of Electrical and Computer Engineering at Nation University of Singapore in 2008–2009. Currently he is an assistant professor in Institute of Photonics at National Changhua University of Education, Changhua City, Taiwan. He is also a visiting scholar of the Department of Electrical and Computer Engineering at Nation University of Singapore now. His research interests include photonic crystals, phononic crystals and optical MEMS.

Chengkuo Lee (S'93–M'96) received the M.S. degree in materials science and engineering from National Tsing Hua University, Hsinchu, Taiwan, R.O.C., in 1991, the M.S. degree in industrial and system engineering from Rutgers University, New Brunswick, NJ, in 1993, and the Ph.D. degree in precision engineering from the University of Tokyo, Tokyo, Japan, in 1996. He worked as foreign researcher in the Nanometerscale Manufacturing Science Laboratory at the Research Center for Advanced Science and Technology (RCAST) of the University of Tokyo from 1993 to 1996. He had also worked in the Mechanical Engineering Laboratory, AIST, MITI of Japan as a JST Research Fellow in 1996. Thereafter, he was a Senior Research Staff Member of Microsystems Laboratory, Industrial Technology Research Institute (ITRI), Hsinchu, Taiwan, R.O.C. In September 1997, he joined the Metrodyne Microsystem Corporation, Hsinchu, Taiwan, R.O.C., and established the MEMS device division and the first micromachining fab for commercial purposes in Taiwan. He was the Manager of the MEMS device division between 1997 and 2000. He was an Adjunct Assistant Professor in the Electro-physics Department of National Chiao Tung University, China, in 1998, and an Adjunct Assistant Professor in the Institute of Precision Engineering of the National Chung Hsing University, China, from 2001 to 2005. He co-founded Asia Pacific Microsystems, Inc. (APM) Hsinchu, Taiwan, R.O.C., in August 2001, and he became the Vice President of R&D, then later until the end of 2005, the VP of optical communication business unit and Special Assistant of CEO in charge of international business and technical marketing for MEMS foundry service at APM, Inc., one of the top 30 MEMS manufacturers in the world in 2004. From 2006 to 2009, he has been a senior member of technical staff at the Institute of Microelectronics (IME), A-Star, Singapore. He has been an assistant professor at the Department of Electrical and Computer Engineering of National University of Singapore, Singapore since December 2005. He is the co-author of a book in title of Advanced MEMS Packaging, McGraw-Hill, 2010. He has contributed more than 120 international conference papers and extended abstracts, 70 peer-reviewed international journal articles, and 8 US patents in MEMS, Nanophotonics and Nanotechnology fields. Dr. Lee is the member of the Materials Research Society (MRS), and the Institution of Electrical Engineers (IEE) Japan.

Wenfeng Xiang received the B.Sc. degree from the Department of Physics at the Shandong Normal University, Jinan, China in 2000 and the PhD. degree in materials science and engineering from Institute of Physics, Chinese Academy of Sciences, Beijing, China, in 2005. He worked as post doctor in the Department of Materials Science and Engineering at Gwang-Ju Institute of Science and Technology, Gwang Ju, Korea, from August 2005 to August 2006. He had also worked as Research Fellow in the School of Electrical and Electronic Engineering at Nanyang Technological University from September 2006 to December 2007. He is currently a Research Fellow in the Department of Electrical and Computer Engineering at National University of Singapore, Singapore. His research interests include optical MEMS, nanophotonics sensor, and optical communications.

W.K. Choi received the B.Sc. and PhD degrees in electrical engineering in 1982 and 1986, MBA degree in 1991 from the University of Edinburgh, U.K., respectively. From 1986 to 1991, he was with the Edinburgh Microfabrication Facility, University of Edinburgh, as a Research Fellow. In 1991, he joined the Department of Electrical and Computer Engineering in the National University of Singapore (NUS), where he is currently a Professor. He is the Programme Co-Chair of the Advanced Materials for Micro- and Nano- System trust in the Singapore-MIT Alliance Programme, a Visiting Professor of the Materials Science and Engineering Department of MIT and the Supervisor of the Microelectronics Laboratory at NUS. His research interests are in the synthesis of nano-scale structures for electronic and biomedical applications. He has published over 140 journal papers, 2 book chapters, 95 conference papers and holds over 9 patents